POLITECNICO DI TORINO
Repository ISTITUZIONALE

Polyphenols-derived epoxy vitrimers for smart applications: Electrical conductivity, Joule heating, and strain sensing

Original
Polyphenols-derived epoxy vitrimers for smart applications: Electrical conductivity, Joule heating, and strain sensing / Sesia, R., Gomez Sanchez, J., Collado, I., Cortes, A., Jimenez-Suarez, A., Hakkarainen, M., Spriano, S., Ferraris, S., Sangermano, M.. - In: POLYMER. - ISSN 0032-3861. - ELETTRONICO. - 338:(2025). [10.1016/j.polymer.2025.129044]

Availability:
This version is available at: 11583/3003067 since: 2025-09-15T14:09:15Z

Publisher:
Elsevier

Published
DOI:10.1016/j.polymer.2025.129044

Terms of use:

This article is made available under terms and conditions as specified in the corresponding bibliographic description in the repository

Publisher copyright

(Article begins on next page)

26 November 2026

Polymer 338 (2025) 129044



Contents lists available at ScienceDirect

Polymer

journal homepage: www.elsevier.com/locate/polymer

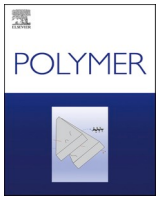

Polyphenols-derived epoxy vitrimers for smart applications: Electrical conductivity, Joule heating, and strain sensing

Rossella Sesia [a,*], Javier Gomez Sanchez [b], Ignacio Collado [a,b], Alejandro Cortes [b], Alberto Jimenez-Suarez [b,c], Minna Hakkarainen [d], Silvia Spriano [e], Sara Ferraris [e], Marco Sangermano [e]

[a] Department of Management and Production Engineering, Politecnico di Torino, C.so Duca degli Abruzzi 24, 10129, Torino, Italy
[b] Materials Science and Engineering Area, University Rey Juan Carlos, C/Tulipán s/n, 28933, Madrid, Spain
[c] Instituto de Investigación de Tecnologías para la Sostenibilidad, Universidad Rey Juan Carlos, C/Tulipán s/n, 28933, Madrid, Spain
[d] Department of Fibre and Polymer Technology, KTH Royal Institute of Technology, Teknikringen 56-58, SE-100 44, Stockholm, Sweden
[e] Department of Applied Science and Technology, Politecnico di Torino, C.so Duca degli Abruzzi 24, 10129, Torino, Italy

ARTICLE INFO

Keywords:
Polyphenols
Carbon nanotubes
Vitrimers
Electrical conductivity
Joule effect heating
Structural health monitoring

ABSTRACT

Epoxy resins play a crucial role in several industrial applications. However, their irreversible crosslinked structure and need for precursors from fossil-fuels provide sustainability issues. This study explores the synthesis of bio-based epoxy vitrimers using glycidylated derivatives of gallic acid (GGA) and tannic acid (GTA) as eco-friendly alternatives. ATR-FTIR and NMR spectroscopies confirmed the successful glycidylation reaction. The thermal curing of epoxy monomers with Vitrimax imine T130 was performed after thoughtful DSC and TGA analyses, achieving reprocessable and thus recyclable materials. Indeed, thanks to the covalent adaptable networks (CANs) based on imine bonds the reprocessing of polyphenols-based composites was possible by hot-pressing their powders after a grinding step. Carbon nanotubes (CNT) were introduced into natural polyphenol-based materials at 1 and 2 wt% contents to improve electrical conductivity and piezoresistive properties. Thermomechanical performance of the bio-based composites was assessed as a function of CNT content, measuring a glass transition temperature of approximately 60 °C. Electrical conductivity measurements revealed an outstanding capability of polyphenols-based composites to conduct electricity with a percolation threshold at 1 wt% of CNT, reaching a maximum of 0.1 S/m and 0.4 S/m for GGA and GTA, respectively. Moreover, unlike systems with 1 wt%, the composites with 2 wt% of CNT exhibited significant Joule heating capabilities reaching 60 °C by just applying about 50 V. Finally, strain-sensing tests demonstrated the electro-mechanical responsiveness of the composites, showing outstanding gauge factors of 89 and 17 with the GGA_1CNT and GTA_1CNT, respectively, highlighting their potential in structural health monitoring (SHM) applications. This work underscores the feasibility of electrically conductive natural polyphenol-based composites as sustainable, recyclable, and multifunctional alternatives to conventional epoxy systems.

1. Introduction

Among the most widely exploited thermosetting polymers, the applications of epoxy resins span to various industrial fields, such as coatings, adhesives, electronic encapsulation, and matrices for advanced composites [1]. Epoxy resins account for approximately 70 % of the global share of the thermoset market (excluding polyurethanes) [2]. However, the chemical industry is nowadays moving towards a greener chemistry to adopt sustainable development principles due to the unsustainable exploitation of fossil-fuels resources. Therefore, attention to renewable resources for the synthesis of bio-based compounds is significantly growing, as they can represent alternatives to epoxies from Bisphenol A (BPA) [2,3]. Many investigations have focused on the exploitation of bio-based epoxy materials, like vegetable oil derivatives [4–6]. Nevertheless, natural aromatic phenols, particularly tannins or their constituents, are rarely considered in research [7–9]. Since aromatic compounds are widely used in industry to develop rigid and thermally stable materials, due to their notable properties related to

* Corresponding author.
E-mail address: rossella.sesia@polito.it (R. Sesia).

https://doi.org/10.1016/j.polymer.2025.129044
Received 15 May 2025; Received in revised form 27 August 2025; Accepted 6 September 2025
Available online 8 September 2025
0032-3861/© 2025 The Authors. Published by Elsevier Ltd. This is an open access article under the CC BY license (http://creativecommons.org/licenses/by/4.0/).

π-stacking interactions [10], natural polyphenols are potential green substitutes for epoxy aromatic resins from fossil-fuels sources [11]. Indeed, polyphenols represent the largest family of secondary plant metabolites, including phenolic acids and tannins, and one of the most ubiquitous compounds in terrestrial biomass [12,13]. Major sources of polyphenols are primarily plants, particularly their soft tissues such as leaves, needles, or bark from various tree species [14,15]. Additionally, natural phenolic compounds can be extracted from by-products of the agri-food industry, including peels and seeds [15–17]. Finally, the high reactivity of phenolic groups towards several chemical reactions is exhaustively reported in literature [11,18–20]. In detail, the OH groups in natural polyphenols have proven suitable for the glycidylation reaction, as demonstrated by Tomita et al. patent, which represents the most industrially used procedure to develop polyphenols-based epoxy monomers [21].

Moreover, traditional epoxy resins cannot be reprocessed, recycled, or repaired due to their permanently crosslinked molecular structures. Various approaches, including covalent adaptable networks (CANs) [1, 22–24], dynamers [25] or vitrimers [26] have been employed to develop innovative repairable, recyclable, and/or reprocessable epoxy-based materials. These types of epoxy resins have shown significant potential as matrices for micrometric and nanometric carbon-based reinforcements, like carbon nanotubes, carbon black, carbon nanofibers and graphene nanoplatelets [1,27,28]. The incorporation of these reinforcements substantially enhances mechanical, electrical, piezoresistive and thermal properties [29–31], as well as improves or introduces additional functionalities, such as Joule heating, self-healing, and shape memory [32–35].

In this framework, carbon nanotubes (CNT) have proved to effectively increase the aforementioned properties, also allowing the development of multifunctional nanocomposites [22,31,32]. CNT have been demonstrated to be highly suitable as fillers for polymer nanocomposites in advanced material applications [36], in particular by exploiting bio-based monomers as a matrix [37,38]. Different works have been addressed by our research group on the development of carbon nanofillers-doped bio-based polymers, like polyglycerol-based acrylic compounds [39], diglycidylether of vanillyl alcohol [31] and acrylated epoxidized soybean oil with isobornyl methacrylate [40], highlighting the possibility of fabricating highly electrically conductive materials. Moreover, epoxidized castor oil has been demonstrated to be an optimal matrix for reprocessable and reshapable CNT-reinforced composites. Indeed, Bergoglio et al. combined the vitrimeric behaviour due to the thermo-activated transesterification reaction and the incorporation of CNT to achieve bio-based, recyclable, and electrically conductive composites [41].

A key application of CNT-doped materials is in structural health monitoring (SHM). SHM enables real-time assessment of structural integrity, including the detection, localization, and quantification of strain and damage, as well as the prediction of the structure's remaining useful life [42]. CNT-doped composites exhibit significant potential in this field, primarily due to the intrinsic piezoresistive properties of CNT [43,44], the contact-based conductive mechanisms between them, and the tunnelling effect between adjacent nanotubes. These combined factors provide higher strain sensitivity, noticeably exceeding that of conventional metallic strain gauges [44,45].

Within this frame, in the present work, gallic and tannic acids, two natural polyphenols, were functionalized to obtain bio-based epoxy monomers to be used as composite matrices. The thermal curing of these synthesized bio-based epoxy compounds was performed with the commercial Vitrimax imine T130 hardener resin, obtaining circularly recyclable and reprocessable CANs. CNT were added to achieve nanocomposites with high electrical conductivity and Joule effect performance. Finally, the strain-sensing capabilities of these natural polyphenol-based composites were assessed under tensile load conditions. By means of this approach, the optimal combination of mechanical and electrical properties can be identified and tailored to desired application requirements.

2. Materials and methods

2.1. Materials

The natural extract of tannic acid (TA) from *Caesalpina spinosa* was supplied by Silvateam (San Michele Mondovì, Italy). Gallic acid (GA), tetrabutylammonium bromide (TBAB, 98 %), epichlorohydrin (ECH), and sodium hydroxide (NaOH) were purchased from Sigma-Aldrich. Acetone (≥99.5 %), Dimethylsulfoxide-d6 (DMSO-d_6, purity of 99.8 %), chromium(III)-2,4-pentanedionate ($Cr(acac)_3$, 97 %), 2-chloro-4,4,5,5-tetramethyl-1,3,2-dioxaphospholane (TMDP, 95 %) and pyridine (anhydrous, 99.8 %) were purchased from Sigma Aldrich. N-Hydroxy-5-norbornene-2,3-dicarboxylic acid imide (NHND, >99.0 %) was purchased from Tokyo Chemical Industry. NC7000 multiwalled carbon nanotubes (CNT) with an average length of 1.5 μm and an outer diameter of 9.5 nm were supplied by Nanocyl (Sambreville, Belgium). The Vitrimax imine T130 hardener resin was purchased from Mallinda (Denver, Colorado, USA), and chloroform-d (99.8 %) from Cambridge Isotope Laboratories.

2.2. Glycidylation reaction of gallic acid and tannic acid

The glycidylation reaction of GA and TA with ECH was carried out following a method described for commercially available resins [21,46]. The polyphenol (3.0 g) was mixed with ECH (15.0 g), TBAB (0.30 g) and distilled water (10.0 g) for 30 min at room temperature. Then, the suspension was stirred at 80 °C for 1 h. Afterwards, 20 mL of 20 % aqueous solution of NaOH was slowly added to the reaction mixture through a constant pressure dropping funnel. The resulting mixture was stirred for 3.5 h at 80 °C, and subsequently diluted with an excess of acetone (about 100 mL), filtered and vacuum concentrated at 80 °C to remove the unreacted ECH and residual solvent. Thus, the glycidylated gallic acid (GGA) and tannic acid (GTA) were achieved.

2.3. Manufacturing of samples

GGA and GTA systems were manufactured according to an adaptation of Mallinda protocol. Neat GGA and GTA systems were prepared as follows. After degassing the Vitrimax T130 at 70 °C, the glycidylated polyphenol was added to the imine hardener with a 2:1 imine to epoxy mass ratio and mixed at 60 °C. The mixture was poured in a metallic open mold, and thermally cured according to a two-step method: the first curing step was set up at 100 °C for 2 h, whereas the second one at 130 °C for 3 h.

In the case of CNT-doped epoxy systems, a previous dispersion step was included. After heating the monomer at70 °C, CNT were dispersed into the glycidylated polyphenol *via* an ultrasonic probe, a Hielscher UP400S equipment, for 5 min at 50 % amplitude and 0.5 s cycles. The resulting mixture was degassed in vacuum conditions for 20 min before adding the imine hardener. Two concentrations of CNT of 1 wt% and 2 wt% were evaluated.

2.4. Nuclear Magnetic Resonance (NMR) spectroscopy

GA and GGA were characterized by proton nuclear magnetic resonance (^{1}H NMR) spectroscopy at 400 MHz and 25 °C, utilizing a Bruker Avance 400 spectrometer. Dimethylsulfoxide-d6 (DMSO-d_6) was used as the solvent and the internal standard for chemical shift calibration.

The quantitative analysis of OH groups in TA before and after the functionalization was carried out by means of Phosphorus nuclear magnetic resonance (^{31}P NMR), according to a protocol for hydroxyl groups determination [47]. Since tannins have complex chemical structures and their solubility in organic solvents is low, ^{31}P NMR analysis is a strategic method to quantify and distinguish OH groups.

Hence, a phosphorylation reaction of TA and the functionalized TA was necessary, and the chemical shifts of the resulting phosphorylated OH groups were assessed [48,49]. A solution of chloroform-d and anhydrous pyridine with a volume ratio of 1:1.6 (vol/vol) was prepared and named solvent A. About 30 mg of tannin sample was dissolved in 0.5 mL of solvent A. For the internal standard solution, two solutions were prepared in solvent A and then mixed together: 5.0 mg/mL solution of the relaxing agent $Cr(acac)_3$ and 18.0 mg/mL solution of the internal standard NHND. Subsequently, 0.1 mL of the internal standard solution was added to the tannin sample solution. The resulting mixture was stirred overnight. Prior to ^{31}P NMR analysis, 0.1 mL of the phosphorylating agent TMDP was added to the homogenous tannin solution and stirred for 30 s. To perform ^{31}P NMR spectroscopy, the phosphitylated tannin solution was poured into a 5 mm NMR tube, and a Bruker Avance IIII HD 400 MHz spectrometer was used. A relaxation delay of 2 s and 1024 scans were used as acquisition parameters. The resulting NMR data were elaborated through MestReNova software (Mastrelab Research SL), and phase corrections and automatic baseline were applied. The chemical shift was calibrated to the reference signal of the product of TMDP and water at 132.2 ppm. The determination of hydroxy group content on TA and the functionalized TA was evaluated by integrating peak regions attributed to OH groups. In detail, the used integration regions were 149.0–147.0 ppm (aliphatic OH), 144.0–138.8 ppm (phenolic OH) and 133.6–136.0 ppm (carboxylic acid OH) [47,48]. Derived integral values were converted to mmol OH/g tannin in accordance with Equation (1):

$$\text{mmol OH} \Big/ \text{g tannin} = \frac{\text{R} \times \text{NHND in NMR sample}}{\text{Dry weight of tannin}} \quad (1)$$

where R is the integral ratio of the ^{31}P NMR region of interest over the region of the internal standard.

The degree of substitution (DS) was estimated according to Equation (2):

$$\text{DS} = \frac{C(OH)_i - C(OH)_f}{C(OH)_i + C(OH)_f \times \Delta m_{max}} \quad (2)$$

$C(OH)_i$ and $C(OH)_f$ are the initial and final concentrations of OH units (mmol/g) in tannin, respectively, and Δm_{max} is the weight increase per g of tannin at 100 % conversion.

2.5. Fourier Transform Infrared (FTIR) spectroscopy

A PerkinElmer Spectrum 100 spectrometer (PerkinElmer Waltham, Massachusetts, US), equipped with a diamond crystal, was used to investigate the structural changes before and after functionalization of the natural polyphenols. The attenuated total reflection (ATR) mode was exploited. The ATR-FTIR spectra were recorded with a resolution of 4 cm^{-1} as the average of 16 scans.

2.6. Differential Scanning Calorimetry (DSC)

A Mettler-Toledo 882e (Columbus City, OH, USA) equipment was used to perform differential scanning calorimetry (DSC) analyses.

To evaluate the thermal curing conditions of GGA and GTA with the Vitrimax imine hardener, four DSC cycles were carried out with a heating rate of 20 °C/min and under N_2 flow of 50 mL/min. Firstly, the sample was heated from 0 to 100 °C; an isothermal step at 100 °C was performed for 120 min; after that, the temperature increased to 130 °C; lastly, the sample underwent an isothermal step at 130 °C for 60 min. The epoxy conversions of GGA and GTA formulations *via* thermal curing were estimated in accordance with Equation (3) [9]:

$$\text{Conversion degree} = \frac{\Delta H_{exp}}{\Delta H_{dyn}} \times 100 \quad (3)$$

where ΔH_{exp} is the enthalpy measured in the isocuring condition and ΔH_{dyn} is the enthalpy evaluated in the dynamic run performed from 25 to 250 °C, which can theoretically ensure complete curing. Hence, ΔH_{dyn} can be taken as a reference to assess the conversion.

Glass transition temperature (T_g) for the cured GGA and GTA with different CNT content ranging from 0 to 2 wt% was assessed through DSC. The first heating step from 10 to 150 °C was followed by a cooling step to room temperature, with a rate of 5 °C/min and a N_2 flow of 50 mL/min.

2.7. Thermogravimetric analysis (TGA)

The thermal stability of GGA and GTA was studied by thermogravimetric analysis (TGA) by using a Mettler Toledo TGA/DSC1. About 5 mg of the glycidylated sample was placed in 70 μL ceramic crucible and was heated from 30 to 800 °C with a rate of 10 °C/min in an Ar atmosphere (50 mL/min).

2.8. Recycling procedure

The recycling ability of cured GGA and GTA was performed by grinding the samples into fine powder. The resulting powder was pressed and heated between two Kapton films with a CARVER manual press at 130 °C for 15 min with a pressure of 25 kPa.

2.9. Dynamic Mechanical Thermal Analysis (DMTA)

Thermo-mechanical characterization of GGA and GTA systems with different CNT content (0–2 wt%) was performed by using a Q800 DMA instrument (TA Instruments, New Castle, DE, USA). The tests were carried out at 1 Hz in the single cantilever configuration for rectangular specimens of 35 × 12.7 × 1.8 mm^3, from −30 to 100 °C with a rate of 2 °C/min.

2.10. Scanning Electron Microscopy (SEM)

In order to assess the dispersion of CNT in the composites, a microstructural analysis was performed on the fracture surfaces. The samples were coated by sputtering a thin layer of gold and a field emission gun scanning electron microscope (FEG-SEM, Nova NanoSEM 230 from Philips) was used.

2.11. Electrical conductivity and Joule effect heating

The electrical conductivity of GGA and GTA samples with different CNT content (0–2 wt%) was measured following the ASTM D257 standard [50]. A direct current was applied to 10 × 10 × 1 mm^3 specimens by using a Keithley 2410 source-meter from Keithley Instruments (Cleveland, OH, USA). The electrical resistance (R) was determined as the slope of the I–V (intensity *vs* voltage) curve by sweeping the voltage from 0 to 50 V. The electrical conductivity (σ) was calculated according to Equation (4):

$$\sigma = \frac{L}{SR} \quad (4)$$

where L is the distance between the electrodes, and S is the cross-sectional area of the sample. Silver conductive paste was used to minimize the contact resistance between the electrodes and the specimen. The measurements were performed in duplicate.

The above-mentioned source-meter and a FLIR T530 thermal camera from FLIR Systems linked to FLIR Tools + software (v6.4) were used to assess the Joule effect heating. The maximum temperature (T_{max}) was measured as a function of the applied voltage.

2.12. Electromechanical test

Tensile tests were performed to evaluate the electromechanical

behaviour of the manufactured GGA and GTA materials with 1 and 2 wt % of CNT [51]. A Zwick Z100 (Ulm, Germany) universal tensile machine was used. The test was performed on rectangular specimens of 35 × 12.7 × 1.8 mm^3 at a rate of 5 mm/min up to 0.25 %strain, and electrical characterization was carried out simultaneously to the mechanical test by using an Agilent 34410 A module (Santa Clara, CA, USA). The electrical resistance change of the sample between two electrodes of copper wire and silver ink was measured. The electrical sensitivity to the applied strain, or gauge factor (GF), was evaluated as the ratio between the normalized electrical resistance and the applied strain according to Equation (5):

$$GF = \frac{\Delta R/R_0}{\varepsilon} \quad (5)$$

where ΔR is the instantaneous electrical resistance increment with respect to the initial electrical resistance, R_0, and ε is the strain in the sample.

3. Results and discussions

3.1. Synthesis of GGA and GTA

Gallic acid (GA) and tannic acid (TA) were reacted with epichlorohydrin in an alkaline medium to achieve the corresponding glycidylated derivatives with high yields of products, as illustrated in Fig. 1a.

A yield of around 69 % was estimated for the glycidylated gallic acid (GGA), while the glycidylated tannic acid (GTA) was achieved with a yield of 68 %. The GGA and GTA chemical structures are shown in Fig. 1b and c, respectively.

The introduction of the epoxy ring into the chemical structure of GA was confirmed by ATR-FTIR spectroscopy (Fig. 2a). The new signals at 3000-2780 cm^{-1} and 850 cm^{-1} in the GGA spectrum are attributed to the stretches of alkyl C–H and epoxy C–O–C bonds, respectively. Additionally, the blue shift of the C═O signal, together with the presence of the intense peak of the ester COOC stretches at 1204 cm^{-1} in the GGA spectrum, suggested the glycidylation of the carboxylic group.

In the ATR-FTIR spectrum of GTA (Fig. 2b), the decrease in intensity of the O–H band was noteworthy due to the consumption of hydroxy groups in functionalization. The peaks at 3000-2790 cm^{-1} and the shoulder at 850 cm^{-1} corroborated the effective glycidylation reaction of the TA phenols.

As support to ATR-FTIR results, the NMR spectroscopy was performed on GA and TA before and after the glycidylation reaction. GA and its glycidylated derivative were assessed *via* ^{1}H NMR analysis. The ^{1}H NMR spectrum of the pristine GA (Fig. 3a) was characterized by the peaks of hydroxyl-hydrogens of both phenolic and carboxylic groups, named c, d and b. These signals disappeared due to the glycidylation reaction, as can be seen in the ^{1}H NMR spectrum of GGA (Fig. 3b). Moreover, at low chemical shifts in the ^{1}H NMR spectrum of GGA (Fig. 3b) several multiplets were recorded due to the introduction of the epoxy moieties [20,52].

In order to further verify the successful glycidylation of TA together with ATR-FTIR spectroscopy, the chemical structures of TA and GTA were assessed *via* the ^{31}P NMR (Fig. 3c), which allowed an identification and a quantitative analysis of OH groups in complex polyphenols [47]. As shown in Fig. 3c, the ^{31}P NMR spectrum of TA was characterized by the presence of three different regions related to the phenolic (144.0–138.8 ppm), the aliphatic (149.0–147.0 ppm) and carboxylic OH (133.6–136.0 ppm) groups. The presence of the last two regions was attributable to impurities resulting from the extracting process of TA from *Caesalpina spinosa*. However, after the glycidylation reaction of TA, a notable decrease of the area of all alcohol regions was observed in the ^{31}P NMR spectrum of GTA (Fig. 3c). Hence, the TA's hydroxy moieties, especially the phenolic ones, reacted with epichlorohydrin achieving a complete epoxy functionalization. By means of ^{31}P NMR spectroscopy, the quantification of hydroxy groups in TA and GTA and thus the degree of substitution (DS) was possible according to Equations (1) and (2), respectively. The DS of approximately 99 % after the epoxy functionalization of TA corroborated the high effectiveness of the reaction.

3.2. Manufacturing and reprocessability of GGA and GTA composites

The best curing conditions to ensure the complete crosslinking of GGA and GTA by means of the Vitrimax imine T130 hardener addition were identified by means of DSC analyses in dynamic and isothermal curing. The dynamic curing allowed to reach full conversion. In order to find the optimal parameters of time and temperature for manufacturing, isothermal curing was performed to simulate the crosslinking conditions, as Fig. 4a–b illustrate. The conversion degrees of the glycidylated polyphenol formulations are reported in Table 1. For both GGA and GTA monomers, the highest enthalpy (ΔH) value was achieved at 100 °C. Thus, the thermal curing of samples with and without CNT was carried

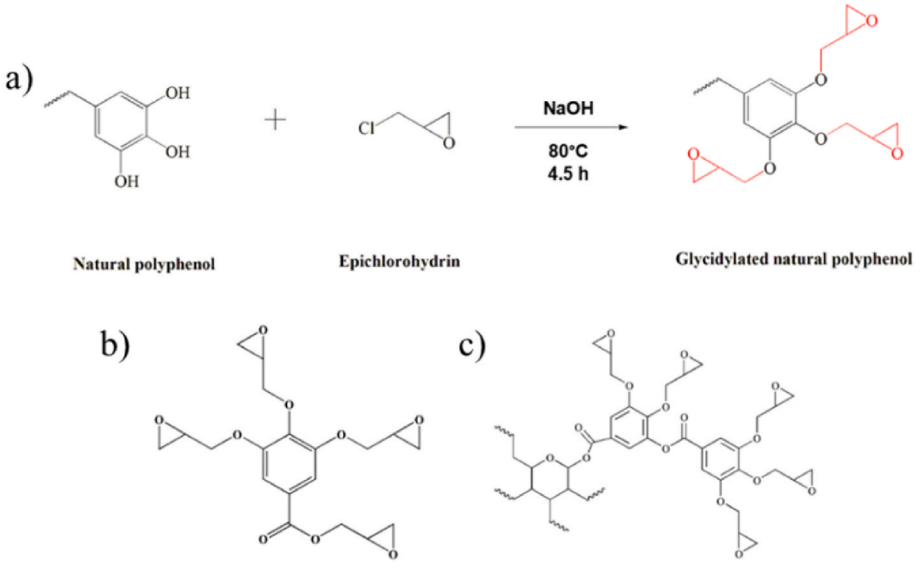

Fig. 1. (**a**) Simplified schematization of the glycidylation reaction of natural polyphenols with epichlorohydrin; (**b**) Chemical structure of GGA; (**c**) simplified chemical structure of GTA.

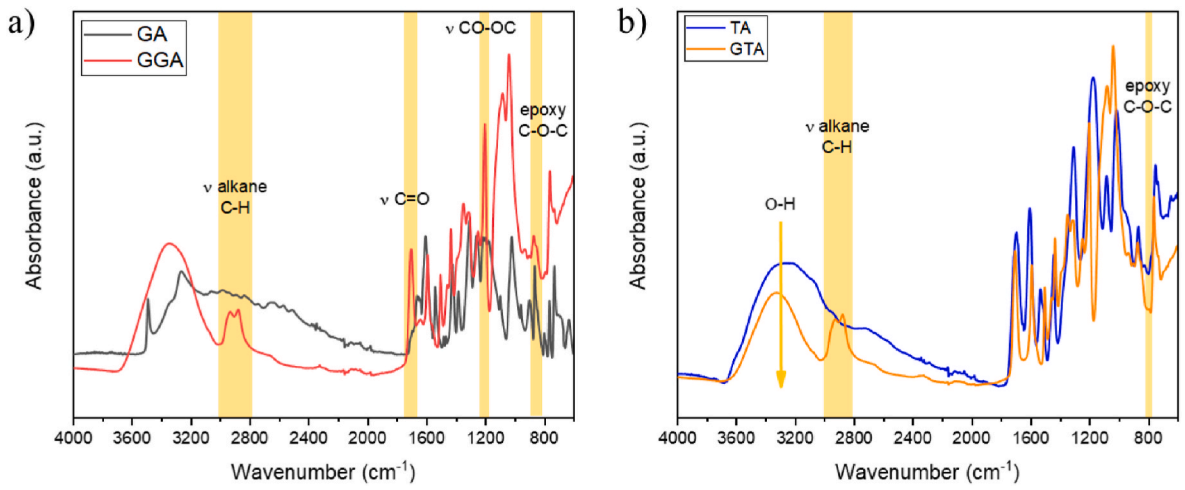

Fig. 2. ATR-FTIR spectra of (**a**) GGA and (**b**) TA before and after glycidylation reaction.

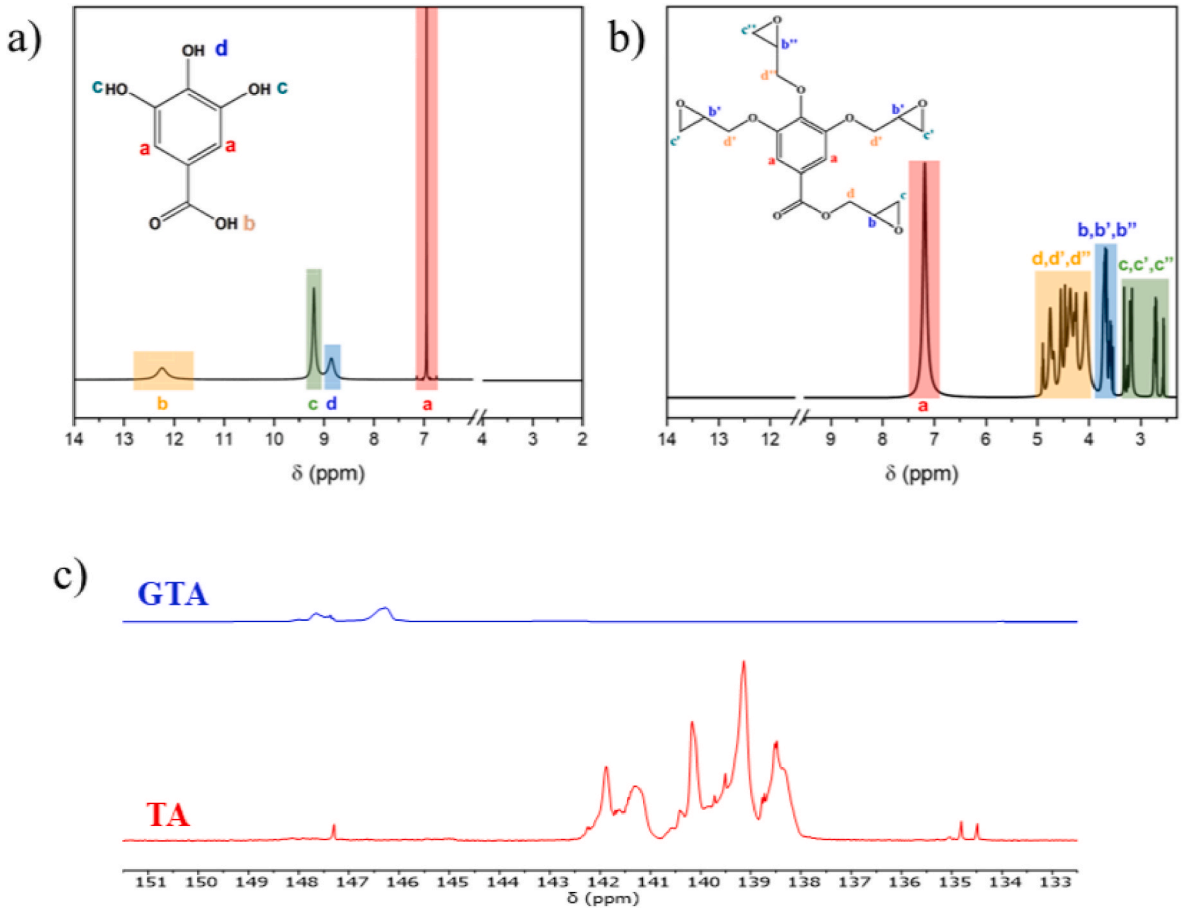

Fig. 3. ^{1}H NMR spectrum of (**a**) GA and (**b**) GGA; (**c**) ^{31}P NMR spectrum of TA before and after glycidylation reaction.

out in a two-step process. The first curing at 100 °C for 2 h was used to initialize the curing process, while the second step at 130 °C for 3 h was used to achieve full conversion.

This thermal curing method was made possible by the considerable thermal stability of the uncured GGA and GTA monomers at the required temperatures. Indeed, as shown by TGA curves in Fig. 4c, both epoxy monomers exhibited a slightly unstable thermal profile. This can probably be ascribed to the water presence from the glycidylation reaction or adsorbed from the atmosphere. At 100 °C, mass losses of 4 % and 5 % were measured for GGA and GTA, respectively, while the mass losses for GGA and GTA were estimated 7 % and 11 % at 130 °C, respectively. Therefore, these values of mass loss were negligible for the curing procedure. The thermal degradation temperature of 20 % mass loss ($T_{deg20\ \%}$) was measured at 246 °C for GGA and at 199 °C for GTA, presumably due to the isomerization of epoxide into aldehydes or the epoxide etherification with the unfunctionalized OH groups [53]. The char yield (w_{char}) of GGA and GTA was approximately 19 % and 18 %, respectively. Given the high thermal stability of the epoxy monomer, the two-step

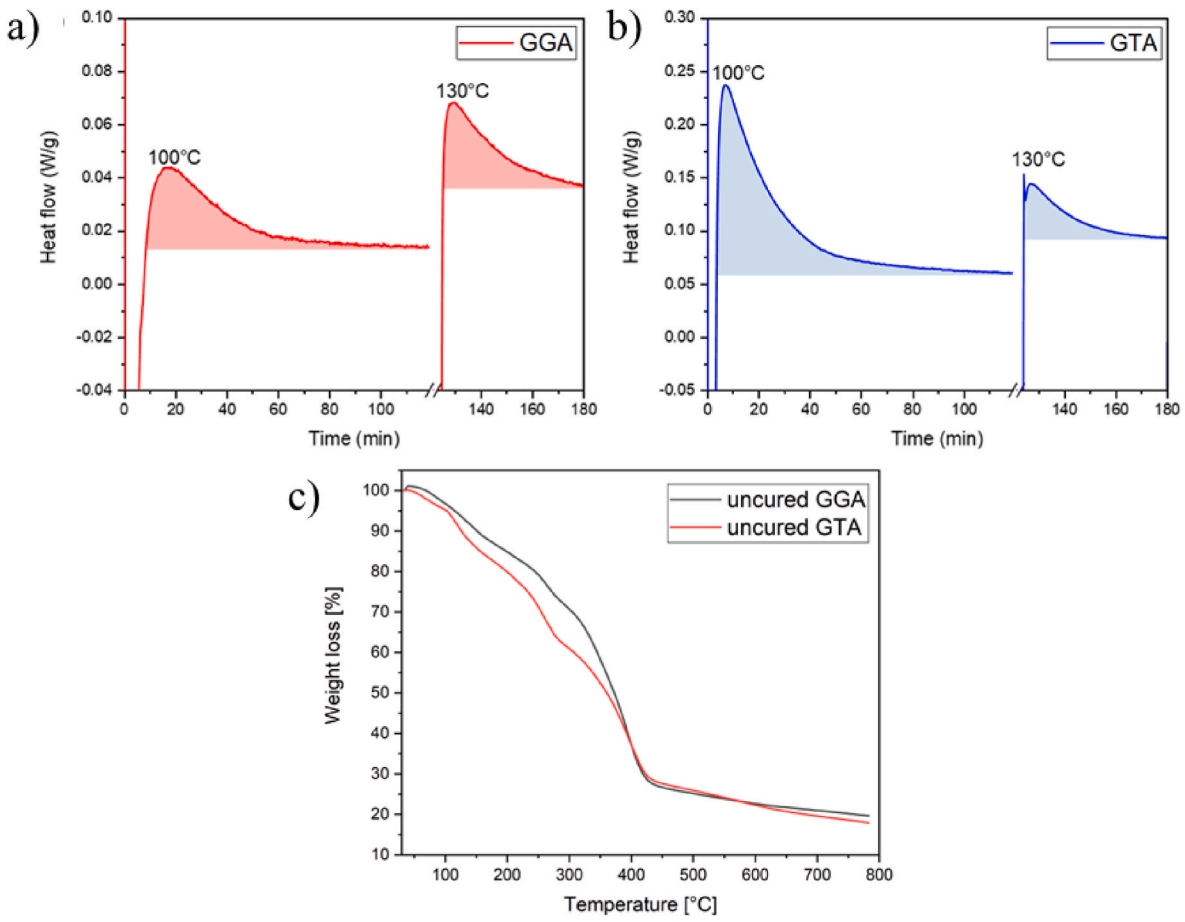

Fig. 4. DSC curves in isothermal curing of (**a**) GGA and (**b**) GTA formulations; (**c**) TGA curve of GGA and GTA monomers.

Table 1
Dynamic and isothermal DSC results of GGA and GTA formulations.

Formulation	ΔH (J/g)[a]	T_{peak} (°C)[a]	T (°C)[b]	ΔH (J/g)[b]
GGA	209.9	134	100	52.68
			130	39.66
GTA	508.2	131	100	181.6
			130	36.01

[a] From the dynamic curing curve.
[b] From the isothermal curing curve.

thermal curing method at 100 and 130 °C was also performed to prepare the CNT-reinforced samples at different concentrations (0.5, 1, and 2 wt %).

Since the curing was carried out with the Vitrimax hardener, which enables reprocessing to change the specimen's shape after curing due to the dynamic bonds within the network, GGA and GTA-based materials proved to be reprocessable, as shown in Fig. 8. This recycling possibility can be explained by the reversible exchange of imine bonds, leading to the rearrangement and reformation of epoxy networks [54,55]. After grinding the original crosslinked composites, the resulting powders were hot-pressed at 130 °C for 15 min with a pressure of 25 kPa, thus obtaining the recycled crosslinked samples shown in Fig. 5.

Therefore, when a part made of the proposed material reaches the end of its useful life or breaks during service, it can be reprocessed using this simple method to produce a part with the same geometry or a completely different one. This demonstrates the sustainability of the proposed materials, which contribute to the circular economy given their reprocessing capabilities.

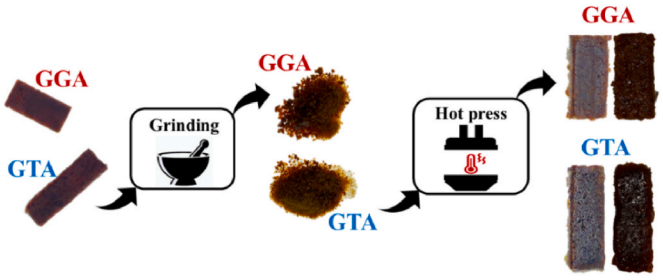

Fig. 5. Schematization of the reprocessing of cured GGA and GTA resins.

3.3. Thermal and thermo-mechanical properties of composites

In order to develop bio-based reprocessable composites with multi-functional properties, like electrical conductivity and strain-sensing capabilities, carbon nanotubes (CNT) were added into GGA and GTA formulations, because they have proven to be efficient fillers for advanced material applications [41]. After the manufacturing of the polyphenols-based nanocomposites, as described in the paragraph 2.3, the thermal properties of the samples were assessed by means of DSC measurements. The DSC curves of cured GGA and GTA pristine samples and composites are reported in Fig. 6a–b, respectively. Analysing the results in detail, the T_g values slightly decreased for both GGA and GTA systems as the CNT content increased (Fig. 6c) due to the influence of CNT on the crosslinking process. Steric hindrance potentially occurred with the resulting reduction in the T_g [22].

The decreasing trend in the T_g when increasing the CNT content was corroborated by DMTA experiments, confirming the effect of the steric

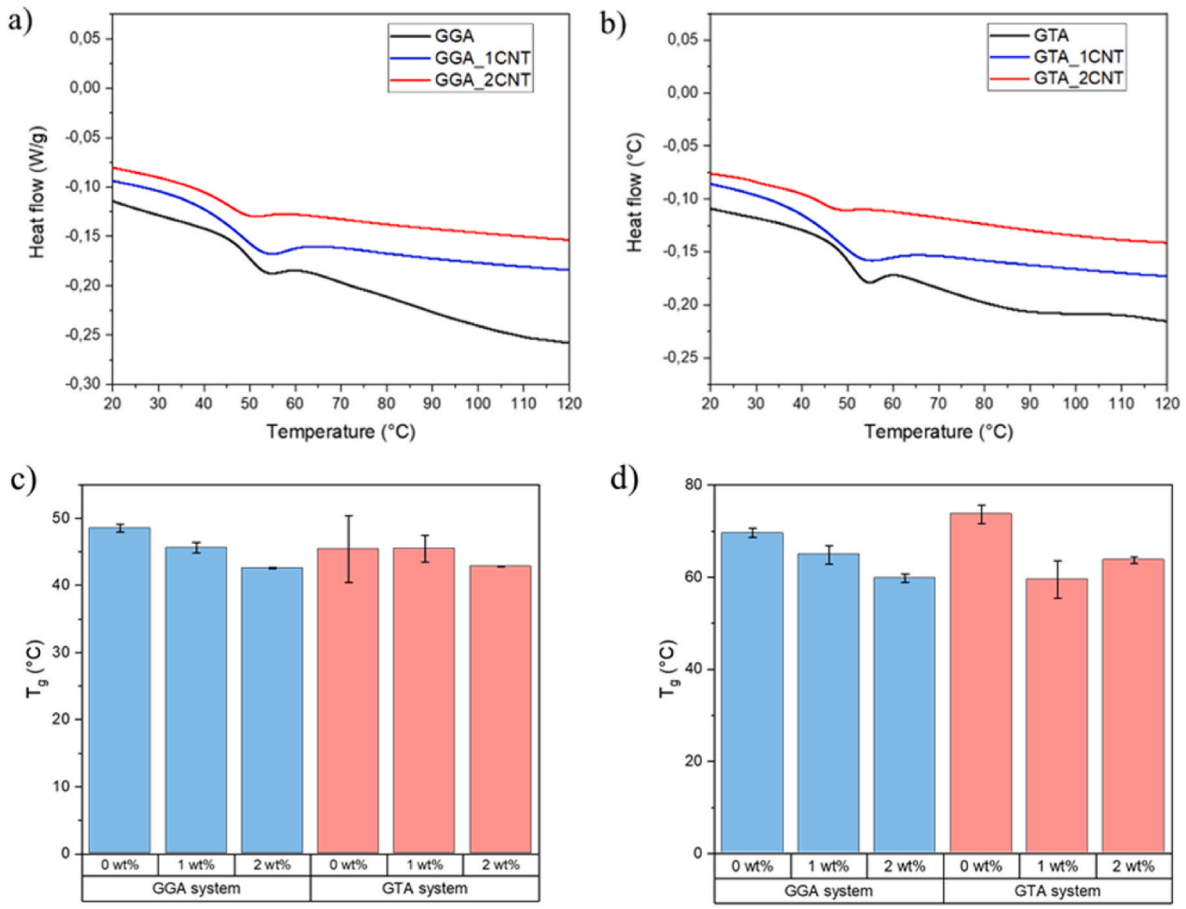

Fig. 6. DSC curves of (**a**) GGA and (**b**) GTA composites with different CNT contents; (**c**) T_g values estimated *via* DSC analysis; (**d**) T_g values estimated *via* DMTA for GGA and GTA composites as a function of CNT content.When comparing the thermomechanical behaviour of the reprocessed specimens (5 times reprocessed) with regard to the original ones, a slight decrease in storage modulus and glass transition temperature can be observed for the reprocessed ones (Fig. 7a and b-c-d).

hindrance. All the data are collected in Fig. 6d for both the polyphenol-based systems. The decrease in T_g was more pronounced among GGA samples, and its modest flexibilization impact could be accounted for the decrease in epoxy group conversion in the presence of CNT [41]. Instead, the T_g values were almost similar between the GTA specimens with the two different CNT contents. This behaviour indicated the energy dissipation characteristics of the GTA composites [32]. The DMTA analyses were also performed on reshaped samples after hot-pressing the ground powder.

More specifically, the storage modulus decreased around 20 % in both GGA and GTA systems for the reprocessed specimens with regard to the original specimens, which can be attributed to the presence of entrapped air between the powder before reprocessing, a lack of reprocessability between adjacent particles due to an ineffective dynamic bond exchange, or due to degradation of the material caused by the high reprocessing temperatures. Moreover, very similar T_g values were achieved after reprocessing the samples, showing the good reprocessability of the polymer network attributed to the presence of Vitrimax imine hardener, which shows dynamic covalent behaviour.

In addition to the DMTA analysis, which is the standard and most widely applied technique to evaluate vitrimer reprocessability, we also performed tensile tests on the composites containing 2 wt% CNTs, both before and after mechanical reprocessing. Fig. S1 of supplementary material shows the tensile tests for both systems reinforced with 2 % CNT. The results show the same trends observed in the DMTA tests performed on the pristine system before and after mechanical reprocessing. In particular, the GTA system shows higher Young's modulus values, i.e., greater stiffness, both before and after reprocessing, but at the same time lower strain at break or lower maximum elongation capacity.

The differences between GTA and GGA are due to their fundamentally different molecular structures. Tannic acid (GTA) is a more complex natural polymer with a branched structure containing multiple gallic acid units esterified to a glucose core, providing more phenolic groups. In contrast, gallic acid (GGA) is a much simpler molecule. This structural difference results in a higher cross-linking density in the case of GTA. The literature confirms that tannic acid generates more densely cross-linked networks than gallic acid, due to its greater functionality (more reactive sites available to form bonds with the Vitrimax imine hardener, the conformational restriction it imposes on the polymer chains, limiting their mobility and increasing rigidity, and the existence of stronger intermolecular interactions, which reinforce the three-dimensional network [56]. Therefore, tannic acid results in more rigid and resistant but less flexible materials, since the presence of multiple phenolic units leads to a more compact and restricted network that significantly limits the segmental mobility of the polymer chains.

In both systems, it can be observed that after reprocessing there is a loss in both stiffness and deformation capacity at break. This degradation of mechanical properties is a common phenomenon in glass-like polymers and is due to several simultaneous factors. First, there is a degradation of the polymer network. As observed in the DMTA results, the decrease in the storage modulus can be attributed to an inefficient dynamic exchange of imine bonds during reprocessing, since not all of them are optimally rearranged, as well as to the possible breakage of permanent covalent bonds under the grinding and re-pressing conditions [57]. Secondly, reprocessing introduces microstructural defects

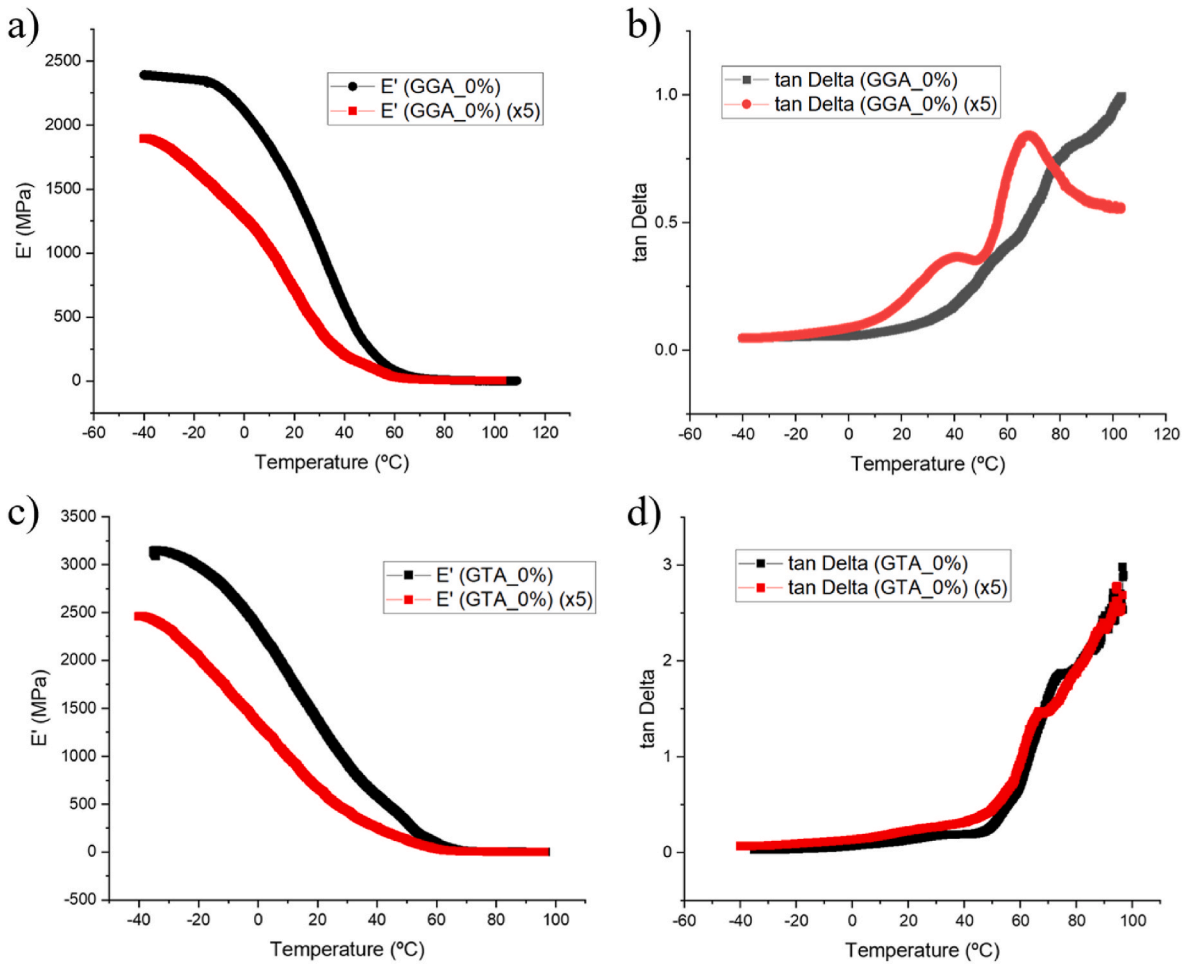

Fig. 7. DMTA as a function of the monomer and reprocessing. (**a**) Storage modulus and (**b**) tan delta of GGA specimens. (**c**) Storage Modulus and (**d**) tan delta of GTA specimens.

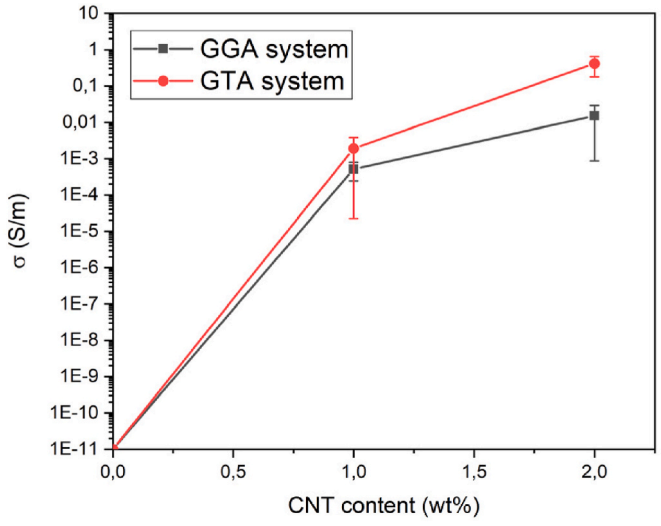

Fig. 8. Electrical conductivity as a function of the CNT content for the GGA and GTA crosslinked polymer networks.

that directly affect mechanical properties [57]. During re-pressing, air is often trapped, which generates microporosity; in addition, adjacent particles do not always fuse completely, resulting in incomplete bonds, and the resulting network is less homogeneous than the original. Thirdly, the specific effects of the presence of CNTs also contribute to the loss of mechanical properties in nanocomposites with 2 % reinforcement. Grinding and reprocessing can break connections between nanotubes, causing partial disruption of the conductive network. Furthermore, CNTs can reorient themselves in a less favorable manner for mechanical load transmission, and the CNT-polymer interface can deteriorate during reprocessing, compromising stress transfer between phases.

Finally, the loss of deformation at break is explained by an increase in brittleness. The microstructural defects introduced act as stress concentrators, reducing the material's resistance to tensile stresses. In addition, the lower molecular mobility of the reprocessed network limits the polymer's ability to accommodate large deformations, while the heterogeneities introduced during reprocessing cause premature failures in poorly bonded areas under load.

3.4. Electrical conductivity analysis

Since the ability of carbon nanofillers to increase electrical performance is well known [34,35], the electrical conductivity (σ) values for the GGA and GTA composites with different content of CNT was assessed and the results are shown in Fig. 8. The σ increased with the CNT amount due to the formation of a higher number of electrically conductive pathways [22,31,32,58]. Both GGA and GTA systems showed outstandingly high σ values, demonstrating the possibility to use natural polyphenols-based matrices for nanocomposites development.

In detail, GTA samples reinforced with 2 wt% of CNT exhibited about

ten times the electrical conductivity of GGA samples with the same CNT content (Fig. 8). This behaviour could be explained by the better dispersion of CNT in the GTA matrix due to more effective π–π interactions between CNT and the large number of aromatic systems in GTA [59]. As can be seen in Fig. 9, the FEG-SEM images suggested a slightly better dispersion of the carbon nanofillers in GTA_2CNT than GGA_2CNT. The formation of some CNT aggregates in GGA_2CNT, highlighted in the SEM image, explained the poorer dispersion and thus the lower σ values. However, the CNT dispersion was overall similar among GGA and GTA specimens (Fig. 9), especially for CNT content of 1 wt%. Indeed, the σ values of GGA_1CNT and GTA_1CNT were measured as comparable, although GTA_1CNT showed a higher standard deviation since it was close to the electrical percolation threshold.

In addition to characterizing the electrical conductivity of the vitrimer after its original manufacture, it is also important to characterize it after several reprocessing cycles. Fig. S2 of supplementary material shows the electrical conductivity values of both systems for 1 % and 2 % CNT by weight, comparing the conditions before and after reprocessing. Fig. S2a shows that the GGA system loses electrical conductivity after reprocessing, regardless of the CNT content. Furthermore, in the case of 2 % CNT, the loss of conductivity is more pronounced after mechanical reprocessing. Fig. S2b shows the same analysis but for the GTA system. In this case, it can be seen that for a CNT content of 1 %, the electrical conductivity remains practically constant, while for 2 % CNT a clear decrease is observed. It is important to note that, overall, the GTA system exhibits better electrical performance after reprocessing.The greater loss of electrical conductivity in the system with 2 % CNT after mechanical reprocessing is mainly due to the breakdown of more complex and dense percolation networks, together with the fact that the increased rigidity of the material increases the probability of irreparable damage to the network. In systems with concentrations close to the percolation threshold (1 % CNT in this case), the conductive network is relatively simple and sparse, and damage and the introduction of defects are less likely, which increases the probability that a larger part of the network will become established. Conversely, at higher concentrations (2 % CNT), more complex secondary and tertiary percolation networks are formed that depend on more numerous contacts, and damage and defects generated during processing are more likely, reducing the probability of re-establishing these networks.

In other words, the grinding and re-pressing process alters dense networks (2 %) more drastically than simpler ones (1 %), leading to more severe connectivity losses. Both DMTA and tensile tests show a reduction in mechanical properties after reprocessing, which is consistent with the presence of microvoids and poorer packing. In 2 % CNT, due to the higher density of CNT-CNT and CNT-matrix contacts, the voids interrupt more conductive pathways and the interfacial layer, which is slightly weaker after reprocessing, thickens the tunnel barrier in a greater number of contacts. The improved performance of the GTA system after mechanical reprocessing can be attributed to the specific characteristics of the tannic acid-based glass network. The results of the DMTA and tensile tests show that both systems (GGA and GTA) experience a decrease in the storage modulus after reprocessing. However, the more flexible and branched structure of tannic acid allows for more effective redistribution of stresses during reprocessing, which helps preserve CNT connectivity by minimizing damage [60]. This same factor also promotes better wetting of CNTs, so that during reprocessing, compaction expels air more easily. By reducing the number of voids, fewer conductive pathways are interrupted.

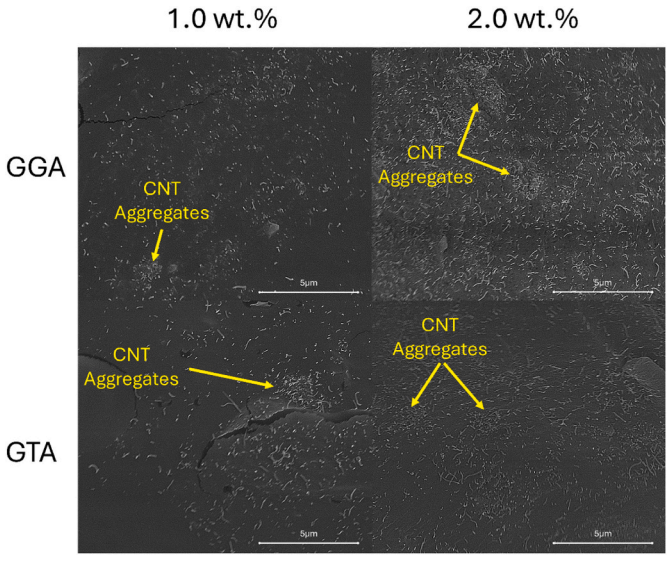

Fig. 9. FEG-SEM images of GGA and GTA composites with different contents of CNT. All images were acquired under identical conditions(HV 5Kv, HFW 14.9um, WD 5.4 mm) at a magnification of 20,000 × .

Another key aspect is that the GTA system, based on tannic acid with multiple phenolic groups, generates a denser and more efficient network of imine bonds. These dynamic covalent bonds reorganize during reprocessing, helping to maintain electrical connectivity [61]. With the same imine curing agent (Vitrimax), the macromolecular architecture of GTA facilitates dynamic exchange and "resealing" of CNT-CNT and CNT-matrix contacts during hot pressing, allowing for better recovery of the percolation network compared to GGA. The more complex chemical structure of tannic acid compared to gallic acid also offers more anchorage points for CNTs, resulting in a more efficient CNT-polymer interface [60]. This reduces the likelihood of nanotube disconnection during mechanical reprocessing. In this regard, the high aromatic density and abundance of phenolic groups in GTA favor both π-π interactions and hydrogen bonding with the graphene surface of the nanotubes, reinforcing anchoring during shearing and preventing loss of contact.

The electrical conductivity performances of these natural polyphenol-based CNT-doped systems were comparable to BPA-based composites [62], and remarkably higher than other bio-based epoxy systems with CNT [63,64]. The electrical percolation threshold was identified as the critical CNT content at which the material transitioned to an electrically conductive state, marked by a sudden increase in σ. Therefore, the electrical percolation threshold was evaluated to be 1 wt % for both systems, consistent with findings from other studies utilizing similar CNT [44].

In addition, advanced quantitative segmentation analysis was performed using the yen threshold algorithm. This method allowed us to clearly highlight the spatial location and aggregation state of CNTs within each micrograph, facilitating reliable visualization and partial reconstruction of the conductive network architecture (see Fig. S3 of supplementary material). Through particle analysis and mathematical filtering of the segmented images (including minimum pixel size thresholds to exclude background noise and sub-resolution features) we quantified the apparent number of CNTs and aggregates in each system. These experimentally derived values were then directly compared to theoretical predictions based on the nominal CNT loading. This comparison enables qualitative and semi-quantitative assessment of dispersion quality and network uniformity across compositions. As shown in Fig. S4 of supplementary material, for the 2 wt% CNT samples, the GGA-2 system exhibits a much greater apparent area occupied by CNTs and more pronounced aggregation compared to GTA-2, indicating the tendency of GGA matrix to promote CNT clustering at higher loadings. In contrast, at 1 wt% CNT, the differences are subtler, although GTA-1 still appears to exhibit a slightly more heterogeneous dispersion than GGA-1. The particle count analysis, scaled to area and supported by theoretical benchmarks, confirms the trends observed in electrical conductivity results, where more homogeneous CNT dispersion in the GTA matrix (especially at higher loading) is associated with improved percolation and conductive network formation.

3.5. Joule effect heating

The addition of carbon nanofillers enables resistive heating through the Joule effect due to the formation of an electrical network throughout the composites. The Joule effect consists of heat dissipation upon the application of an electric field [65,66], and it is directly related to the electrical conductivity [32]. Hence, Joule's heating potential was assessed for both the glycidylated polyphenols systems (Fig. 10a).

As shown in Fig. 10a, the temperature achieved through Joule heating showed trends consistent with the material's σ values. Higher electrical conductivity corresponded to lower electrical resistance (R) for samples of identical length (L) and cross-sectional area (s), as described by Equation (4). Thus, when the same voltage (V) is applied, a higher electrical current (I) is generated according to Ohm's law (Equation (6)).

$$V = I \times R \tag{6}$$

An increase in the amount of heat released *via* Joule heating (Q) occurred, in accordance with Joule's law (Equation (7)), where t represents time of voltage application [22,32].

$$Q = I^2 \times V \times t \tag{7}$$

Furthermore, the highest resistive heating capabilities were measured for GGA and GTA materials with 2 wt% of CNT due to their higher σ values. As can be seen in Fig. 10a, the voltage required to achieve the glass transition temperature of approximately 60 °C for GGA_2CNT and GTA_2CNT was about 50 V, while higher voltages were needed for GGA_1CNT and GTA_1CNT (330 V and 350 V, respectively). Thermographs of the composites with the highest Joule heating capability CNT content (2 wt% of CNT for both GGA and GTA formulations) are shown in Fig. 10b. The recorded thermographs revealed a relatively uniform heating across the samples due to the homogenous distribution of CNT, and suggested the possibility of reprocessing the polyphenol-based vitrimers *via* the Joule heating effect. Joule heating cyclic stability tests were performed prior to the measurements presented in Fig. 10 in order to ensure reproducibility and reliability. Each sample was subjected to two consecutive heating–cooling cycles, after which no significant changes in the maximum temperature or heating rate were detected. All subsequent data were recorded once the system had stabilized. This confirms that the Joule heating response is highly stable for maximum temperatures up to 130 °C, which is consistent with the curing protocol (final step of 3 h at 130 °C) and indicates that no structural rearrangements are expected within this thermal window.

3.6. Structural health monitoring

The mechanical and strain-sensing performances of the GGA and GTA vitrimers were influenced by the carbon nanofiller's addition. These properties were assessed in tensile conditions on the samples with 1 and 2 wt% CNT.

The normalized electrical resistance increased for all investigated composites as the strain increased during axial tensile tests due to the growing interparticle distance between adjacent CNT in the polymeric network. CNT-doped materials are capable of effectively monitoring strain progression and detecting damage onset within the matrix in real time [67]. Fig. 11 shows the electrical ($\Delta R/R_0$) and mechanical (σ) signal versus percentage strain. In the upper part (Fig. 11a–b), the SHM performed on the GGA system is plotted. A strong nonlinearity in the electrical signal is observed despite the mechanical signal showing a linear trend. The lower part (Fig. 11c and dd) shows that the GTA system presents a more linear electrical signal, which follows the trend of its mechanical signal. The nonlinear behaviour of GGA specimens can be attributed to the effect of the tensile clamps on the regions close to the electrodes [68]. This effect is not present in the GTA specimens because this system is stiffer than GGA. Another explanation could be that the GTA percolation network shows a more homogeneous structure with respect to the GGA one [69].

Table 2 shows the GF values for an interval between 0 and 0.25 % strain and an interval from 0.1 to 0.2 % strain. This is intended to show the dependence of the GF on the strain and on the existence of pre-strain (assuming an initial 0.1 % strain). In the second row of results (Table 2), linearity was assumed between 0.1 and 0.2 % strain, which is realistic if a preload inducing a strain of 0.1 % is applied, which would linearize the electrical response of all studied conditions.

Analysing the results in detail, a higher GF is observed for the specimens reinforced with the lowest CNT content (1 wt%), regardless of the matrix used, since the CNT content is closer to the electrical percolation threshold (see Fig. 8), where the tunnelling effect is more prevalent [70]. Under these conditions, the percolating network consists of weak connections (electronic tunnels) between dispersed CNT, which are easily broken by small deformations [71]. This sudden disconnection of critical paths causes a very sharp increase in relative resistance ($\Delta R/R_0$), resulting in an exceptionally high gauge factor (GF). At 2 wt% CNT, the samples are well above the percolation threshold, implying a dense and highly redundant network with multiple parallel driving paths, being dominant the contact mechanism. In this context, strain affects a lower proportion of critical electrically conductive paths, so the relative electrical resistance variation ($\Delta R/R_0$) is low and, consequently,

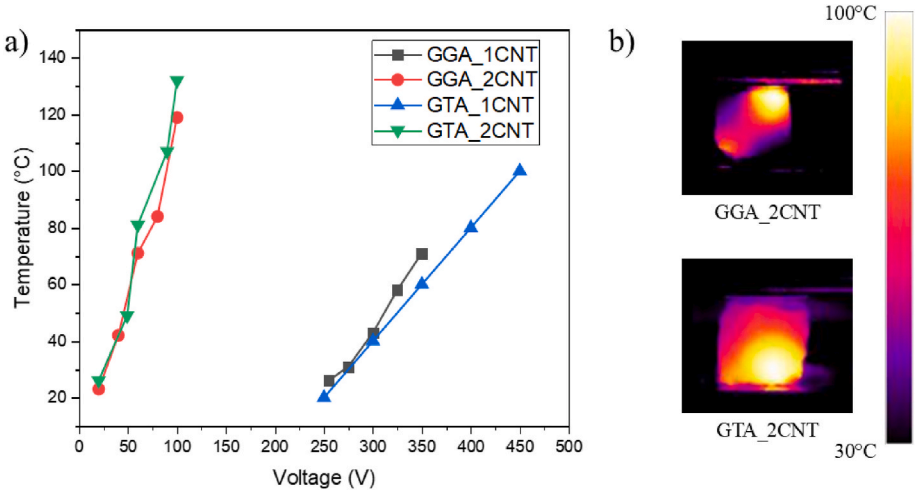

Fig. 10. (**a**) Maximum temperature reached by Joule effect heating as a function of the applied voltage; (**b**) thermograms of GGA and GTA composites with 2 wt% of CNT recorded at 100 V during the Joule effect heating.

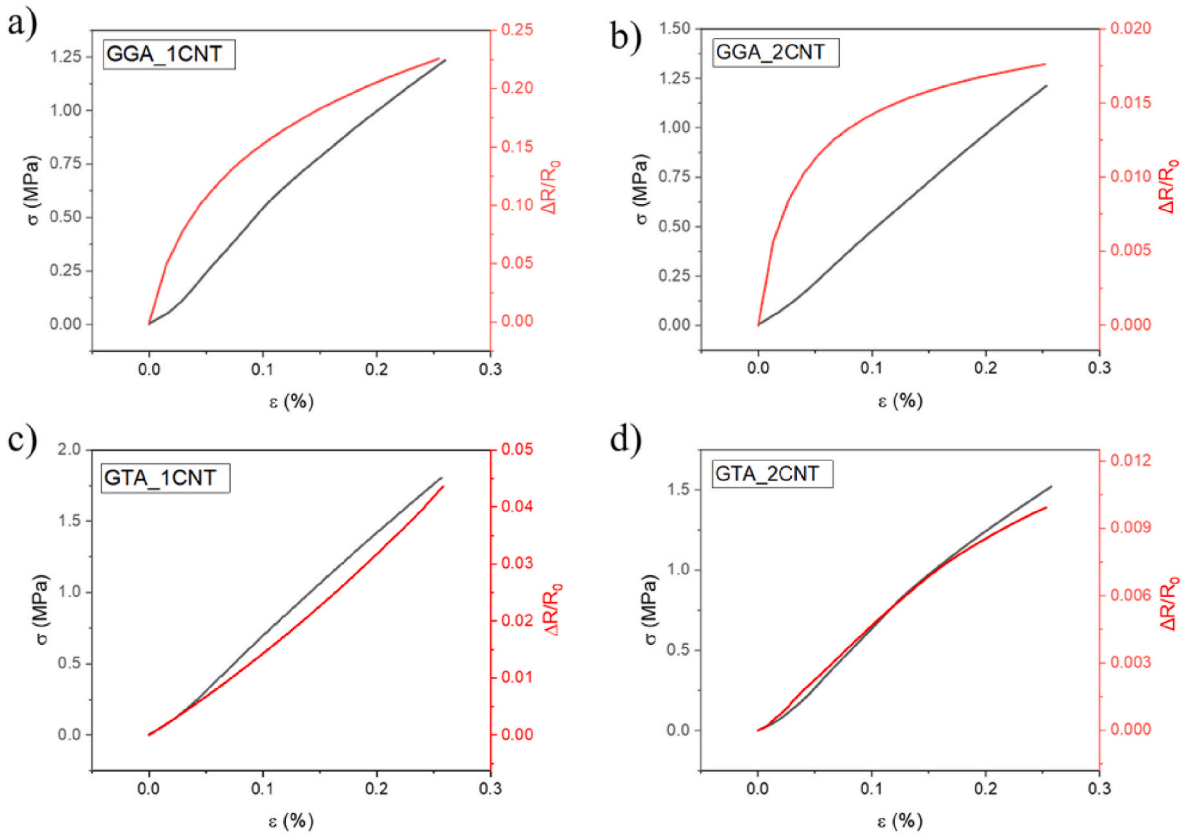

Fig. 11. Structural health monitoring results for the GGA system reinforced **a)** with 1 % CNT and **b)** with 2 % CNT, and the GTA system reinforced **c)** with 1 % CNT and **d)** with 2 % CNT.

Table 2
Gauge Factor (GF) results for the different matrices, contents, and deformation conditions.

Strain conditions	Gauge Factor			
	GGA_1CNT	GGA_2CNT	GTA_1CNT	GTA_2CNT
0.0 % - 0.25 %	88.73	6.99	16.97	3.84
0.1 % - 0.2 %	50.95	3.09	17.24	3.88

the gauge factor (GF) also decreases [72].

Furthermore, GGA systems presented a higher GF than the GTA ones, regardless of the CNT content, which can be attributed to their lower electrical conductivity, closer to the percolation threshold, thus inducing a greater predominance of the tunnelling effect over the contact electrically conductive mechanism [58].

As previously mentioned, significant differences in the GF values are observed for the GGA specimens in the two studied strain ranges (0–25 and 0.1–0.2 % strain). This can be explained by its non-linearity, caused by the tensile clamps, and lower electrical conductivity. The above-mentioned results are demonstrated by observing the variation of the

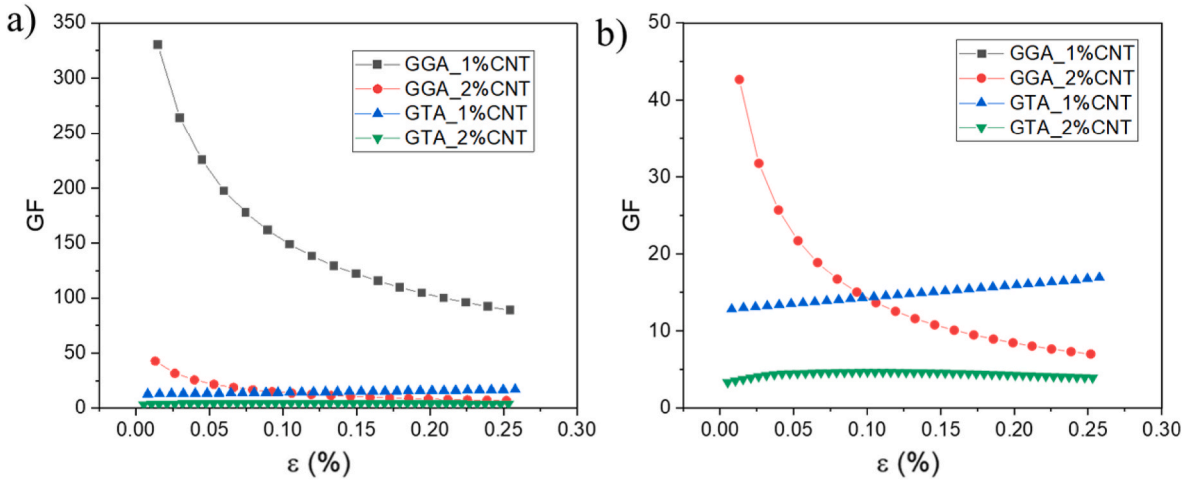

Fig. 12. Results of the instantaneous GF calculation for the different values of deformation tested. Results are shown (**a**) for all systems (matrix with CNT) tested and (**b**) an enlargement at lower GF values (up to 50) to appreciate the dependence of GF on deformation.

instantaneous GF, i.e., the quotient between the $\Delta R/R_0$ and the strain for each strain value [73] (Fig. 12a–b). This plot shows a high variation in GF with the applied strain for the GGA system, while it shows a more stable GF for the GTA one. In the case of GTA, there is a slight growth of the GF for 1 % due to the tunnel effect contributions, while for 2 wt% CNT, it shows a stable behaviour linked to an over-percolated network, located in the driving zone dominated by the contact resistance. It is also shown that at higher deformations the GGA GF tends to stabilize, eliminating the non-linear contribution, which would indicate that the origin of this non-linearity would be the effect of the tensile clamps on the electrode zone (not present in the GTA because it is stiffer than the GGA), or because the GTA percolation matrix or network shows a more homogeneous structure with respect to the GGA [69]. This suggests that the CNT interact better with the GTA system, anchoring themselves more strongly in the matrix.

In summary, the results obtained in the strain-sensing tests, conducted in tensile mode, evince the suitability of the proposed systems for structural health monitoring purposes. More specifically, the GF values obtained with the proposed nanocomposites were significantly higher than the ones obtained with conventional metallic gauges (around 2–3) [74]. Furthermore, unlike conventional metallic gauges, which can only detect strain or damage onset on the structure's surface, the proposed nanocomposites are able to detect strain or damage onset throughout the whole structure since the electrical signal flows through the entire cross-section of the structure.

4. Conclusions

The glycidylation reaction of gallic acid (GA) and tannic acid (TA) was used to successfully generate an epoxy monomer based on natural polyphenols. By adding the commercially available Vitrimax imine T130 hardener, the thermal curing of the glycidylated gallic acid (GGA) and tannic acid (GTA) was examined. These bio-based materials showed vitrimeric behaviour, as evidenced by their reprocessing, which was made possible by the introduction of the imine-based hardener characterized by dynamic covalent properties.

Carbon nanotubes (CNT) were added to GGA and GTA systems in two different contents to produce bio-based composites with improved electrical and piezoresistive capabilities. The introduction of CNT had a minor impact on the thermomechanical and thermal characteristics. Indeed, for both systems, a slight decrease in the glass transition temperature (T_g) was assessed due to the steric hindrance. However, with a percolation threshold of 1 wt% of CNT in both systems, outstanding electrically conductive characteristics were measured. The increased CNT content and thus electrical pathways explained the linear trend of electrical conductivity (σ) as a function of CNT content, reaching a maximum σ of 0.1 S/m and 0.4 S/m for GGA and GTA, respectively. The Joule effect heating of GGA and GTA samples was evaluated, as the CNT incorporation facilitates resistive heating *via* the Joule effect. The composites with 2 wt% of CNT demonstrated the highest resistive heating capability. In contrast to the samples with 1 wt% of CNT, the T_g values for GGA_2CNT and GTA_2CNT were achieved by applying a voltage of 50 V, while the maximum temperature at around 120 °C was reached just by applying a voltage of 100 V. Finally, with an electrical sensitivity (also known as the gauge factor, or GF), which varied according to the amount of CNT, the specimens containing 1 and 2 wt% of CNT showed an exceptional electrical response with the applied strain with gauge factors, which are significantly higher than the conventional metallic strain gauges. The maximum gauge factors were measured approximately 89 and 17 for the composites with the lower CNT content (GGA_1CNT and GTA_1CNT, respectively) from 0 to 0.25 % strain. Thus, it was demonstrated that natural polyphenol-based vitrimers might be used as a matrix for sustainable composite materials with strong electrical conductivity and piezoresistive properties.

CRediT authorship contribution statement

Rossella Sesia: Writing – original draft, Visualization, Methodology, Investigation, Data curation. **Javier Gomez Sanchez:** Writing – review & editing, Visualization, Methodology, Investigation, Data curation. **Ignacio Collado:** Writing – review & editing, Visualization, Methodology, Investigation, Data curation. **Alejandro Cortes:** Writing – review & editing, Methodology, Data curation. **Alberto Jimenez-Suarez:** Writing – review & editing, Resources, Project administration, Conceptualization. **Minna Hakkarainen:** Writing – review & editing, Resources, Project administration, Conceptualization. **Silvia Spriano:** Writing – review & editing, Supervision, Funding acquisition. **Sara Ferraris:** Writing – review & editing, Supervision, Funding acquisition. **Marco Sangermano:** Writing – review & editing, Supervision, Project administration, Funding acquisition, Conceptualization.

Declaration of competing interest

The authors declare that they have no known competing financial interests or personal relationships that could have appeared to influence the work reported in this paper.

Acknowledgments

This paper is part of a project that has received funding from the European Union Horizon2020 research and innovation program under the Marie Skłodowska-Curie grant agreement, No. 101085759 (SURE-Poly). Rossella Sesia, Javier Gomez Sanchez and Ignacio Collado contributed equally to this work. MUR is acknowledged for funding R. Sesia's Ph.D. fellowship (MUR – D.M.1061/2021 – Dottorati di ricerca su tematiche green e dell'innovazione: nuove risorse dal PON Ricerca e Innovazione). Silvateam is acknowledged for the collaboration.

Appendix A. Supplementary data

Supplementary data to this article can be found online at https://doi.org/10.1016/j.polymer.2025.129044.

Data availability

Data will be made available on request.

References

[1] G. Seisdedos, E. Viamontes, E. Salazar, M. Ontiveros, C. Pantea, E.S. Davis, T. Rockward, D. McDaniel, B. Boesl, Assessment and non-destructive evaluation of the influence of residual solvent on a two-part epoxy-based adhesive using ultrasonics, Appl. Sci. 13 (2023) 3883, https://doi.org/10.3390/app13063883.
[2] R. Auvergne, S. Caillol, G. David, B. Boutevin, J.-P. Pascault, Biobased thermosetting epoxy: present and future, Chem. Rev. 114 (2014) 1082–1115, https://doi.org/10.1021/cr3001274.
[3] I. Isarn, I. Collado, A. Jiménez-Suárez, S.G. Prolongo, Analysis of bio-based epoxy resins: impact of amine hardeners on thermal, thermomechanical, optical and electrical properties of epoxidized resveratrol with high Tg, React. Funct. Polym. 205 (2024) 106080.
[4] J.-M. Raquez, M. Deléglise, M.-F. Lacrampe, P. Krawczak, Thermosetting (bio) materials derived from renewable resources: a critical review, Prog. Polym. Sci. 35 (2010) 487–509, https://doi.org/10.1016/j.progpolymsci.2010.01.001.
[5] J. Wan, J. Zhao, X. Zhang, H. Fan, J. Zhang, D. Hu, P. Jin, D.-Y. Wang, Epoxy thermosets and materials derived from bio-based monomeric phenols: transformations and performances, Prog. Polym. Sci. 108 (2020) 101287, https://doi.org/10.1016/j.progpolymsci.2020.101287.
[6] S. Nameer, D.B. Larsen, J.Ø. Duus, A.E. Daugaard, M. Johansson, Biobased cationically polymerizable epoxy thermosets from Furan and fatty acid derivatives, ACS Sustain. Chem. Eng. 6 (2018) 9442–9450, https://doi.org/10.1021/acssuschemeng.8b01817.
[7] I. Faye, M. Decostanzi, Y. Ecochard, S. Caillol, Eugenol bio-based epoxy thermosets: from cloves to applied materials, Green Chem. 19 (2017) 5236–5242, https://doi.org/10.1039/C7GC02322G.
[8] R. Dinu, A. Pidvoronia, U. Lafont, O. Damiano, A. Mija, High performance, recyclable and sustainable by design natural polyphenol-based epoxy polyester

thermosets, Green Chem. 25 (2023) 2327–2337, https://doi.org/10.1039/D2GC04414E.
[9] L. Pezzana, E. Malmström, M. Johansson, V. Casalegno, M. Sangermano, Multiple approaches to exploit ferulic acid bio-based epoxy monomer for green thermoset, Ind. Crops Prod. 212 (2024) 118304, https://doi.org/10.1016/j.indcrop.2024.118304.
[10] F. Ng, G. Couture, C. Philippe, B. Boutevin, S. Caillol, Bio-based aromatic epoxy monomers for thermoset materials, Molecules 22 (2017) 149, https://doi.org/10.3390/molecules22010149.
[11] A. Arbenz, L. Avérous, Chemical modification of tannins to elaborate aromatic biobased macromolecular architectures, Green Chem. 17 (2015) 2626–2646, https://doi.org/10.1039/c5gc00282f.
[12] R. Sesia, S. Spriano, M. Sangermano, S. Ferraris, Natural polyphenols and the corrosion protection of steel: recent advances and future perspectives for green and promising strategies, Metals (Basel) 13 (2023) 1070, https://doi.org/10.3390/met13061070.
[13] S. Mal, D. Pal, Tannins and polyphenols extracted from natural plants and their versatile application, 715–757, https://doi.org/10.1007/978-3-030-54027-2_21, 2021.
[14] Y. Liu, J. Wang, Z. Sun, Aromatic biobased polymeric materials using plant polyphenols as sustainable alternative raw materials: a review, Polymers (Basel) 16 (2024) 2752, https://doi.org/10.3390/polym16192752.
[15] S. Quideau, D. Deffieux, C. Douat-Casassus, L. Pouységu, Plant polyphenols: chemical properties, biological activities, and synthesis, Angew. Chem. Int. Ed. 50 (2011) 586–621, https://doi.org/10.1002/anie.201000044.
[16] D. Liu, S. Meng, Z. Xiang, N. He, G. Yang, Antimicrobial mechanism of reaction products of Morus notabilis (mulberry) polyphenol oxidases and chlorogenic acid, Phytochemistry 163 (2019) 1–10, https://doi.org/10.1016/j.phytochem.2019.03.026.
[17] M. Wang, T. Chen, Q. Wang, Y. Shi, Antioxidant, bacteriostatic and preservative effects of extractable condensed tannins isolated from longan pericarps and seeds, Plants 12 (2023) 512, https://doi.org/10.3390/plants12030512.
[18] R. Sesia, M. Porcarello, M. Hakkarainen, S. Ferraris, S. Spriano, M. Sangermano, Sustainable light-assisted 3D printing of bio-based microwave-functionalized gallic acid, Macromol. Chem. Phys. (2024), https://doi.org/10.1002/macp.202400181.
[19] R. Sesia, P. Pou I Rodríguez, M. Calovi, M. Hakkarainen, S. Rossi, S. Ferraris, S. Spriano, M. Sangermano, Microwave-functionalized natural tannic acid as an anticorrosive UV-curable coating, Polymer (Guildf.) 315 (2024) 127824, https://doi.org/10.1016/j.polymer.2024.127824.
[20] C. Aouf, H. Nouailhas, M. Fache, S. Caillol, B. Boutevin, H. Fulcrand, Multi-functionalization of gallic acid. Synthesis of a novel bio-based epoxy resin, Eur. Polym. J. 49 (2013) 1185–1195, https://doi.org/10.1016/j.eurpolymj.2012.11.025.
[21] H. Tomita, K. Yonezawa, Epoxy resin and process for preparing the same, U.S. Patent 4 (802) (1985) 540.
[22] A. Cortés, X.F. Sánchez-Romate, D. Martinez-Diaz, S.G. Prolongo, A. Jiménez-Suárez, Recyclable multifunctional nanocomposites based on carbon nanotube reinforced vitrimers with shape memory and joule heating capabilities, Polymers (Basel) 16 (2024) 388, https://doi.org/10.3390/polym16030388.
[23] Y. Zhang, L. Zhang, G. Yang, Y. Yao, X. Wei, T. Pan, J. Wu, M. Tian, P. Yin, Recent advances in recyclable thermosets and thermoset composites based on covalent adaptable networks, J. Mater. Sci. Technol. 92 (2021) 75–87, https://doi.org/10.1016/j.jmst.2021.03.043.
[24] C.N. Bowman, C.J. Kloxin, Covalent adaptable networks: reversible bond structures incorporated in polymer networks, Angew. Chem. Int. Ed. 51 (2012) 4272–4274, https://doi.org/10.1002/anie.201200708.
[25] N. Roy, B. Bruchmann, J.-M. Lehn, DYNAMERS: dynamic polymers as self-healing materials, Chem. Soc. Rev. 44 (2015) 3786–3807, https://doi.org/10.1039/C5CS00194C.
[26] D. Montarnal, M. Capelot, F. Tournilhac, L. Leibler, Silica-like malleable materials from permanent organic networks, Science 334 (1979) 965–968, https://doi.org/10.1126/science.1212648, 2011.
[27] A. Ruiz de Luzuriaga, R. Martin, N. Markaide, A. Rekondo, G. Cabañero, J. Rodríguez, I. Odriozola, Epoxy resin with exchangeable disulfide crosslinks to obtain reprocessable, repairable and recyclable fiber-reinforced thermoset composites, Mater. Horiz. 3 (2016) 241–247, https://doi.org/10.1039/C6MH00029K.
[28] Y. Wang, Y. Wang, B. Wan, B. Han, G. Cai, Z. Li, Properties and mechanisms of self-sensing carbon nanofibers/epoxy composites for structural health monitoring, Compos. Struct. 200 (2018) 669–678, https://doi.org/10.1016/j.compstruct.2018.05.151.
[29] S. Olhan, B. Antil, V. Khatkar, B.K. Behera, Mechanical, thermal, and viscoelastic behavior of sisal fibre-based structural composites for automotive applications: experimental and FEM analysis, Compos. Struct. 322 (2023) 117427, https://doi.org/10.1016/j.compstruct.2023.117427.
[30] G. Gonzalez, A. Chiappone, I. Roppolo, E. Fantino, V. Bertana, F. Perrucci, L. Scaltrito, F. Pirri, M. Sangermano, Development of 3D printable formulations containing CNT with enhanced electrical properties, Polymer (Guildf.) 109 (2017) 246–253, https://doi.org/10.1016/j.polymer.2016.12.051.
[31] D. Moraru, A. Cortés, D. Martinez-Diaz, S.G. Prolongo, A. Jiménez-Suárez, M. Sangermano, Sustainable electrically conductive bio-based composites via radical-induced cationic frontal photopolymerization, Polymers (Basel) 16 (2024) 2159, https://doi.org/10.3390/polym16152159.
[32] J. Gómez-Sánchez, X.X. Fernández Sánchez-Romate, A. Jiménez-Suárez, S. G. Prolongo, Self-healing activation by conventional resistive heating through the addition of carbon nanotubes in epoxy systems based on covalent adaptable networks, ACS Appl. Polym. Mater. 6 (2024) 1106–1115, https://doi.org/10.1021/acsapm.3c01022.
[33] I. Collado, A. Vázquez-López, S. Heredia, J. de la Vega, A. Jiménez-Suárez, D. Maestre, S.G. Prolongo, Electromagnetic interference shielding of a sequential dual-curing thiol-epoxy system reinforced with GNPs with high shape memory, ACS Appl. Mater. Interfaces (2025), https://doi.org/10.1021/ACSAMI.5C02049/SUPPL_FILE/AM5C02049_SI_002.PDF.
[34] I. Collado, A. Vázquez-López, M. Fernández, J. de la Vega, A. Jiménez-Suárez, S. G. Prolongo, Nanocomposites of sequential dual curing of thiol-epoxy systems with Fe3O4 nanoparticles for remote/in situ applications: thermomechanical, shape memory, and induction heating properties, Adv. Compos. Hybrid Mater. 8 (2025) 1–21, https://doi.org/10.1007/S42114-025-01264-7/FIGURES/10.
[35] L. Simonini, H. Mahmood, A. Dorigato, A. Pegoretti, Evaluation of self-healing capability of a polycaprolactone interphase in epoxy/glass composites, Compos. Part A Appl. Sci. Manuf. 169 (2023) 107539.
[36] J. Fan, Z. Shi, M. Tian, J. Wang, J. Yin, Unzipped multiwalled carbon nanotube Oxide/multiwalled carbon nanotube hybrids for polymer reinforcement, ACS Appl. Mater. Interfaces 4 (2012) 5956–5965, https://doi.org/10.1021/am301623t.
[37] I. Babahan-Bircan, I. Demirkaya, S.O.H. Hasan, J. Thomas, M.D. Soucek, Comparison of new bio-based epoxide-amine coatings with their nanocomposite coating derivatives (graphene, CNT, and fullerene) as replacements for BPA, Prog. Org. Coating 165 (2022) 106714, https://doi.org/10.1016/j.porgcoat.2022.106714.
[38] J. Guo, J. Long, D. Ding, Q. Wang, Y. Shan, A. Umar, X. Zhang, B.L. Weeks, S. Wei, Z. Guo, Significantly enhanced mechanical and electrical properties of epoxy nanocomposites reinforced with low loading of polyaniline nanoparticles, RSC Adv. 6 (2016) 21187–21192, https://doi.org/10.1039/C5RA25210E.
[39] M. Porcarello, S. Bonardd, G. Kortaberria, Y. Miyaji, K. Matsukawa, M. Sangermano, 3D printing of electrically conductive objects with biobased polyglycerol acrylic monomers, ACS Appl. Polym. Mater. 6 (2024) 2868–2876, https://doi.org/10.1021/acsapm.3c03073.
[40] C. Mendes-Felipe, R. Cofano, A. Garcia, M. Sangermano, S. Lanceros-Mendez, Photocurable 3D printed anisotropic electrically conductive materials based on bio-renewable composites, Addit. Manuf. 78 (2023) 103867, https://doi.org/10.1016/j.addma.2023.103867.
[41] M. Bergoglio, G. Palazzo, D. Reisinger, M. Porcarello, G. Kortaberria, S. Schlögl, M. Sangermano, Cationic UV-curing of bio-based epoxidized Castor oil vitrimers with electrically conductive properties, React. Funct. Polym. 200 (2024) 105936, https://doi.org/10.1016/j.reactfunctpolym.2024.105936.
[42] Q. Zheng, B. Han, J. Ou, NanoComposites for structural health monitoring, in: Nanotechnology in Eco-Efficient Construction, Elsevier, 2019, pp. 227–259, https://doi.org/10.1016/B978-0-08-102641-0.00011-6.
[43] M.F. Arif, S. Kumar, T.K. Gupta, K.M. Varadarajan, Strong linear-piezoresistive-response of carbon nanostructures reinforced hyperelastic polymer nanocomposites, Compos Part A Appl Sci Manuf 113 (2018) 141–149, https://doi.org/10.1016/j.compositesa.2018.07.021.
[44] A. Cortés, X.F. Sánchez-Romate, A. Jiménez-Suárez, M. Campo, A. Ureña, S. G. Prolongo, Mechanical and strain-sensing capabilities of carbon nanotube reinforced composites by digital light processing 3D printing technology, Polymers (Basel) 12 (2020) 975, https://doi.org/10.3390/polym12040975.
[45] R. Daňová, R. Olejnik, P. Slobodian, J. Matyas, The piezoresistive highly elastic sensor based on carbon nanotubes for the detection of breath, Polymers (Basel) 12 (2020) 713, https://doi.org/10.3390/polym12030713.
[46] N. Esmaeili, M. Vafayan, A. Salimi, M.J. Zohuriaan-Mehr, Kinetics of curing and thermo-degradation, antioxidizing activity, and cell viability of a tannic acid based epoxy resin: from natural waste to value-added biomaterial, Thermochim. Acta 655 (2017) 21–33, https://doi.org/10.1016/j.tca.2017.06.005.
[47] X. Meng, C. Crestini, H. Ben, N. Hao, Y. Pu, A.J. Ragauskas, D.S. Argyropoulos, Determination of hydroxyl groups in biorefinery resources via quantitative 31P NMR spectroscopy, Nat. Protoc. 14 (2019) 2627–2647, https://doi.org/10.1038/s41596-019-0191-1.
[48] F. Melone, R. Saladino, H. Lange, C. Crestini, Tannin structural elucidation and quantitative 31P NMR analysis. 2. Hydrolyzable tannins and proanthocyanidins, J. Agric. Food Chem. 61 (2013) 9316–9324, https://doi.org/10.1021/jf401664a.
[49] J. Zieher, I. Melikhov, M. Bacher, H. Hettegger, A. Potthast, T. Rosenau, Gallic acid derivatives as stabilizers in cellulose solutions: analysis by 31P NMR spectroscopy, Cellulose 30 (2023) 6109–6118, https://doi.org/10.1007/s10570-023-05275-9.
[50] ASTM International, Test Methods for DC Resistance or Conductance of Insulating Materials, D2vols. 57–14, ASTM, 2021, p. E1, https://doi.org/10.1520/D0257-14R21E01, 2021.
[51] ASTM International, Test Method for Tensile Properties of Plastics, D638, ASTM, 2014, https://doi.org/10.1520/D0638-14.
[52] H. Nouailhas, C. Aouf, C. Le Guerneve, S. Caillol, B. Boutevin, H. Fulcrand, Synthesis and properties of biobased epoxy resins. part 1. Glycidylation of flavonoids by epichlorohydrin, J. Polym. Sci. Polym. Chem. 49 (2011) 2261–2270, https://doi.org/10.1002/pola.24659.
[53] L. Lee, Mechanisms of thermal degradation of phenolic condensation polymers. II. Thermal stability and degradation schemes of epoxy resins, J. Polym. Sci. 3 (1965) 859–882, https://doi.org/10.1002/pol.1965.100030303.
[54] M. Ciaccia, S. Di Stefano, Mechanisms of imine exchange reactions in organic solvents, Org. Biomol. Chem. 13 (2015) 646–654, https://doi.org/10.1039/C4OB02110J.
[55] J.H. Emon, M.A. Rashid, MdA. Islam, MdN. Hasan, M.K. Patoary, Review on the synthesis, recyclability, degradability, self-healability and potential applications of reversible imine bond containing biobased epoxy thermosets, Reactions 4 (2023) 737–765, https://doi.org/10.3390/reactions4040043.

[56] M. Hosseini, L. Moghaddam, L. Barner, S. Cometta, D.W. Hutmacher, F. Medeiros Savi, The multifaceted role of tannic acid: from its extraction and structure to antibacterial properties and applications, Prog. Polym. Sci. 160 (2025) 101908, https://doi.org/10.1016/J.PROGPOLYMSCI.2024.101908.
[57] N. Lorenz, W.E. Dyer, B. Kumru, High-performance vitrimer entailing renewable plasticizer engineered for processability and reactivity toward composite applications, ACS Appl. Polym. Mater. 7 (2025) 1934–1946, https://doi.org/10.1021/ACSAPM.4C03731/ASSET/IMAGES/LARGE/AP4C03731_0003.JPEG.
[58] I. Collado, A. Jiménez-Suárez, A. Vázquez-López, G. Del Rosario, S.G. Prolongo, Ultrasonication influence on the morphological characteristics of graphene nanoplatelet nanocomposites and their electrical and electromagnetic interference shielding behavior, Polymers (Basel) 16 (2024).
[59] E.M. Pérez, N. Martín, π–π interactions in carbon nanostructures, Chem. Soc. Rev. 44 (2015) 6425–6433, https://doi.org/10.1039/C5CS00578G.
[60] Z. Guo, W. Wang, Z. Liu, Y. Xue, H. Zheng, K. Majeed, B. Zhang, F. Zhou, Q. Zhang, Preparation of carbon nanotube-vitrimer composites based on double dynamic covalent bonds: electrical conductivity, reprocessability, degradability and photo-welding, Polymer (Guildf.) 235 (2021) 124280, https://doi.org/10.1016/J.POLYMER.2021.124280.
[61] J. Zhang, Z. Lei, S. Luo, Y. Jin, L. Qiu, W. Zhang, Malleable and recyclable conductive MWCNT-vitrimer composite for flexible electronics, ACS Appl. Nano Mater. 3 (2020) 4845–4850, https://doi.org/10.1021/ACSANM.0C00902/ASSET/IMAGES/LARGE/AN0C00902_0004.JPEG.
[62] I. Collado, A. Vázquez-López, A. Jiménez-Suárez, S.G. Prolongo, Dual-curing MWCNT nanocomposites for energy-efficient electroactive shape memory and In-Situ processing, Chem. Eng. J. 515 (2025) 163471, https://doi.org/10.1016/J.CEJ.2025.163471.
[63] L. Yue, G. Pircheraghi, S.A. Monemian, I. Manas-Zloczower, Epoxy composites with carbon nanotubes and graphene nanoplatelets – dispersion and synergy effects, Carbon N Y 78 (2014) 268–278, https://doi.org/10.1016/j.carbon.2014.07.003.
[64] N. Faggio, F. Olivieri, I. Bonadies, G. Gentile, V. Ambrogi, P. Cerruti, Bio-based epoxy resin/carbon nanotube coatings applied on cotton fabrics for smart wearable systems, J. Colloid Interface Sci. 670 (2024) 337–347, https://doi.org/10.1016/j.jcis.2024.05.062.
[65] Y.S. Song, J.R. Youn, Influence of dispersion states of carbon nanotubes on physical properties of epoxy nanocomposites, Carbon N Y 43 (2005) 1378–1385, https://doi.org/10.1016/j.carbon.2005.01.007.
[66] X. Zhi, J. Liu, H.-B. Zhang, S. Hong, Z.-Z. Yu, Simultaneous enhancements in electrical conductivity and toughness of selectively foamed polycarbonate/polystyrene/carbon nanotube microcellular foams, Compos. B Eng. 143 (2018) 161–167, https://doi.org/10.1016/j.compositesb.2018.01.022.
[67] A. Esmaeili, C. Sbarufatti, A. Jiménez-Suárez, A. Urena, A.M. Hamouda, Piezoresistive characterization of epoxy based nanocomposites loaded with SWCNTs-DWCNTs in tensile and fracture tests, Polym. Compos. 41 (2020) 2598–2609, https://doi.org/10.1002/PC.25558.
[68] M. Nankali, N.M. Nouri, M. Navidbakhsh, N. Geran Malek, M.A. Amindehghan, A. Montazeri Shahtoori, M. Karimi, M. Amjadi, Highly stretchable and sensitive strain sensors based on carbon nanotube–elastomer nanocomposites: the effect of environmental factors on strain sensing performance, J. Mater. Chem. C Mater. 8 (2020) 6185–6195, https://doi.org/10.1039/D0TC00373E.
[69] Y. Fang, L.Y. Li, S.H. Jang, Piezoresistive modelling of CNTs reinforced composites under mechanical loadings, Compos. Sci. Technol. 208 (2021) 108757, https://doi.org/10.1016/J.COMPSCITECH.2021.108757.
[70] Y. Wang, Y. Fu, Z. Meng, B. Wan, B. Han, Experimental study and piezoresistive mechanism of electrostatic self-assembly of carbon nanotubes–carbon black/epoxy nanocomposites for structural health monitoring, J. Mater. Sci. 57 (2022) 12416–12437, https://doi.org/10.1007/S10853-022-07402-6/FIGURES/18.
[71] B. De Vivo, P. Lamberti, G. Spinelli, V. Tucci, Numerical investigation on the influence factors of the electrical properties of carbon nanotubes-filled composites, J. Appl. Phys. 113 (2013), https://doi.org/10.1063/1.4811523/138507.
[72] J. Cha, J. Kim, S. Ryu, S.H. Hong, Comparison to mechanical properties of epoxy nanocomposites reinforced by functionalized carbon nanotubes and graphene nanoplatelets, Compos. B Eng. 162 (2019) 283–288, https://doi.org/10.1016/J.COMPOSITESB.2018.11.011.
[73] L. Vertuccio, L. Guadagno, G. Spinelli, P. Lamberti, V. Tucci, S. Russo, Piezoresistive properties of resin reinforced with carbon nanotubes for health-monitoring of aircraft primary structures, Compos. B Eng. 107 (2016) 192–202, https://doi.org/10.1016/J.COMPOSITESB.2016.09.061.
[74] V. Giurgiutiu, Structural health monitoring (SHM) of aerospace composites, in: Polymer Composites in the Aerospace Industry, Elsevier Ltd, 2015, pp. 449–507, https://doi.org/10.1016/B978-0-85709-523-7.00016-5.